Part II. Discontinuous Galerkin Method Applied to a Single Phase Flow in Porous Media

Beatrice Riviere   Mary Fanett Wheeler   Carlos Baumann

Abstract

This paper is a continuation of a paper written on three methods using discontinuous approximation spaces to solve elliptic problems. The discontinuous Galerkin method is implemented in different cases. Numerical convergence rates are given for smooth and non smooth solutions. The method is applied to two realistic cases of single phase flow in porous media. Error estimation is also numerically studied.

1 Introduction

The dicontinuous Galerkin method considered in this paper was first formulated by Baumann and Oden in [3], [5]. The motivation for the applying the discontinuous Galerkin procedure for modeling flow in porous media arises from the fact that this algorithm is conservative element by element and that higher order approximations which vary locally can by employed. Unlike the locally conservative mixed finite element method no additional functions such as gradients and complicated higher order approximation methods need to be incorporated into the formulation. In addition, the solution of the discretized system is not the solution of a saddle point problem and the number of unknowns can be significantly less. For example in three dimensions to obtain an $O(h^2)$ result, the mixed finite element method requires $108N^3$ unknowns compared to $10N^3$ unknowns for DG. Also in contrast with many of the locally conservative control volume schemes which are vertex centered, the discontinuous Galerkin method does not require two different grids. Some of the features of the discontinuous Galerkin include

- the use of unstructured grids and high order approximation
- full tensor diffusion terms with discontinuous coefficients
- hp adaptivity

Another interesting feature of this method is that an unusual polynomial space can be chosen for quadrilaterals: the $\mathbf{P}_k$ space. This space is well suited for triangular elements but it has been shown that optimal approximation results still hold for quadrilateral elements. Thanks to the discontinuity inherent to the method, such space is possible, and the number of unknowns is less important than in the $\mathbf{Q}_k$ space.

2 Definition of the Problem

2.1 Recall: Some Notations

In this paper, the notations are the ones used in Part 1. Some of the definitions are recalled below. Let Ω be a convex polygonal domain in $\mathbb{R}^n, n = 1, 2, 3$ and let $\mathcal{E}_h = \{E_1, E_2, \ldots, E_{N_h}\}$ be a nondegenerate quasiuniform subdivision of Ω, where E_j is a triangle or a quadrilateral. The finite element subspace is taken to be

$$\mathcal{D}_r(\mathcal{E}_h) = \prod_{j=1}^{N_h} P_r(E_j)$$

where $P_r(E_j)$ denotes the set of polynomials of degree (total) less than or equal than r on E_j if E_j is a triangle or a quadrilateral. We introduce the following H_0^1 norm, for $\phi \in H^1(\mathcal{E}_h)$,

$$|\!|\!|\phi|\!|\!|^2 = \sum_{j=1}^{N_h} (K\nabla\phi, \nabla\phi)_{E_j} + (\alpha\phi, \phi)_{E_j}$$

2.2 Problem and Variational Formulation

The following elliptic problem is considered:

$$\begin{aligned} -\nabla \cdot (K\nabla p) + \alpha p &= f \text{ in } \Omega \\ p &= p_0 \text{ on } \Gamma_D \\ K\nabla p \cdot \nu_N &= g \text{ on } \Gamma_N \end{aligned} \tag{1}$$

where the boundary of the domain, $\partial\Omega$, consists of two disjoint subsets Γ_D and Γ_N. We denote ν_D (respectively ν_N) the unit normal vector to each edge of Γ_D (respectively Γ_N) exterior to Ω. $K = (k_{ij})_{i,j}$ is a full tensor, with each k_{ij} bounded below by a positive constant. We assume that $p \in H^{\frac{1}{2}}(\Gamma_D)$ and $g \in L^2(\Gamma_N)$. If we assume that the k_{ij} are Lipschitz continuous and $f \in L^2(\Omega)$, then the problem (1) has a unique solution in $H^1(\Omega)$ when $\Gamma_D \neq \emptyset$. On the other hand, when $\partial\Omega = \Gamma_N$, the problem (1) has a solution in $H^1(\Omega)$ which is unique up to an additive constant, if f satisfies $\int_\Omega f = 0$. There is a constant C such that

$$||p||_{2,\Omega} \leq C\{||f||_{0,\Omega} + ||p||_{0,\Omega}\}$$

for all $p \in H^2(\Omega)$ solution of (1).

We will consider the non-symmetric bilinear form:

$$\begin{aligned} a_{NS}(\varphi, \phi) &= \sum_{j=1}^{N_h} \left[(K\nabla\varphi, \nabla\phi)_{E_j} + (\alpha\varphi, \phi)_{E_j} \right] \\ &\quad - \sum_{k=1}^{P_h} \int_{e_k} \{K\nabla\varphi \cdot \nu_k\} [\phi] + \sum_{k=1}^{P_h} \int_{e_k} \{K\nabla\phi \cdot \nu_k\} [\varphi] \\ &\quad - \int_{\Gamma_D} (K\nabla\varphi \cdot \nu_D)\phi + \int_{\Gamma_D} (K\nabla\phi \cdot \nu_D)\varphi \end{aligned}$$

We define the linear form:

$$L(\phi) = (f, \phi) + \int_{\Gamma_D} (K\nabla\phi \cdot \nu_D) p_0 + \int_{\Gamma_N} \phi g$$

The discontinuous Galerkin approximation P^{DG} satisfies the formulation

$$a_{NS}(P^{DG}, v) = L(v), \qquad \forall v \in \mathcal{D}_r \tag{2}$$

The fact that this scheme is consistent with the problem (1) has been shown by Baumann [3]. We can show that (2) has a unique solution. In the numerical experiments described in the following section, α is set to be zero.

3 Numerical Experiments

3.1 Convergence rates for a test problem

We introduce the following test problem. $\Omega = (-1, 1)^2$. The exact solution is given by

$$p_{ex}(x, y) = e^{-(x^2+y^2)}, \quad (x, y) \in \Omega.$$

The domain Ω is decomposed into four quadrilateral elements. The permeability tensor will be piecewise constant and defined as below

$$\begin{aligned} K_{11}(x, y) = K_{22}(x, y) &= \begin{cases} 1, & \forall x > 0, \quad y \in (-1, 1) \\ a, & \forall x \leq 0, \quad y \in (-1, 1) \end{cases} \\ K_{12}(x, y) = K_{21}(x, y) &= 0, \quad (x, y) \in \Omega \end{aligned}$$

We assume pure Neumann boundary conditions. We compute the convergence rates in the H_0^1-norm for different values of a and for different orders of approximations. For $a = 1$, we have a uniform material, and the numerical convergence rates are optimal. For the rough coefficient cases, the convergence rates are still optimal.

For a uniform material, the convergence rates in the H_0^1 norm are shown in Table 1. h_0 corresponds to the maximum of the diameters of the elements in the coarse mesh.

For a heterogeneous material, the convergence rates in the H_0^1 norm are shown in Table 2, Table 3. The plot of the error versus the number of degrees of freedom is shown on Fig.2. We note that $\|p_{ex}\| = 1.48815$.

	$r=2$	$r=3$	$r=4$	$r=5$
$h_0/2$	1.53	2.39	3.40	4.82
$h_0/4$	1.65	2.74	3.96	4.97
$h_0/8$	1.86	2.88	3.98	
$h_0/16$	1.95	2.95		

Table 1: Convergence rates for uniform material $a = 1$.

	$r=2$	$r=3$	$r=4$	$r=5$
$h_0/2$	1.76	2.73	3.73	5.09
$h_0/4$	1.85	2.89	4.10	5.01
$h_0/8$	1.96	2.92	4.02	
$h_0/16$	2.00	2.97		

Table 2: Convergence rates for heterogeneous material $a = 10$.

	$r=2$	$r=3$	$r=4$	$r=5$
$h_0/2$	2.05	2.67	4.41	6.01
$h_0/4$	2.16	3.24	4.58	5.49
$h_0/8$	2.23	3.29	4.31	5.27
$h_0/16$	2.22	3.26	4.15	

Table 3: Convergence rates for heterogeneous material $a = 100$.

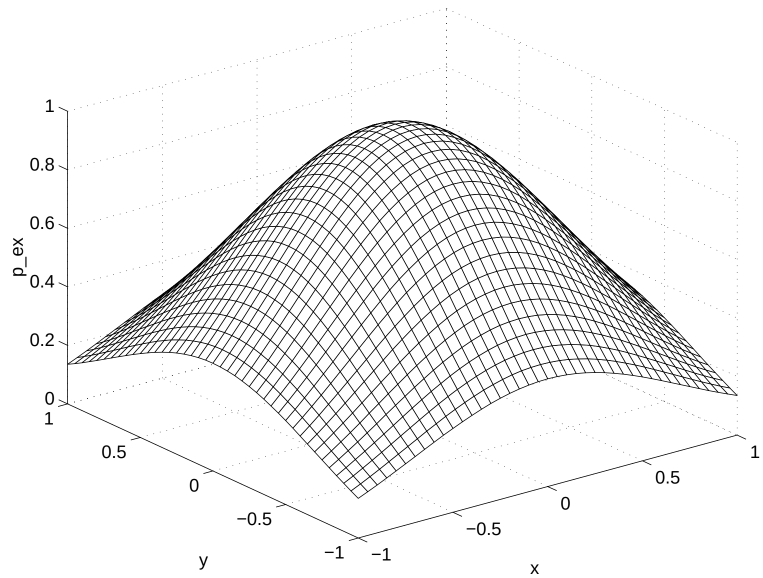

Figure 1: Exact solution.

3.2 Fluid flow in an ash-fly pond

We simulated the flow in the geological L-site, that is located in the south-eastern United States. The L-site consists of a large fly ash disposal pond located adjacent to a river. A cross section is given in Fig.3. There are five different types of rocks. The hydraulic conductivity ranges from 0.31m/day to 17.2m/day.

First, we solve the problem on a coarse mesh with a quadratic approximation. The boundary conditions are the following: no flow on the top and bottom boundaries, and Dirichlet boundary conditions on the vertical boundaries. We impose a constant pressure at the inlet that is higher than the one at the outlet. The Fig.4 shows the computed pressure field. Second, an *hp* adaptive procedure is applied. The mesh is locally refined, and the approximation orders vary elementwise. The pressure and velocity fields are shown in Fig.5. As expected, the flow is more important in the regions where the permeability is higher.

3.3 Fluid flow in a fractured rock

This case consists of two permeable fracture zones intersecting each other. A more detailed description can be found in [4]. The two inclined fracture zones have higher hydraulic conductivity than the surrounding rock. The fracture zones intersect one another at depth. We assume that the medium is isotropic, i.e. $K(\boldsymbol{x}) = k(\boldsymbol{x})I$ for all $\boldsymbol{x} \in \Omega$, where k is a scalar. The value of k in the fracture zones and the surrounding rocks are $10^{-6}ms^{-1}$ and $10^{-8}ms^{-1}$, respectively. We assume no-flow boundary

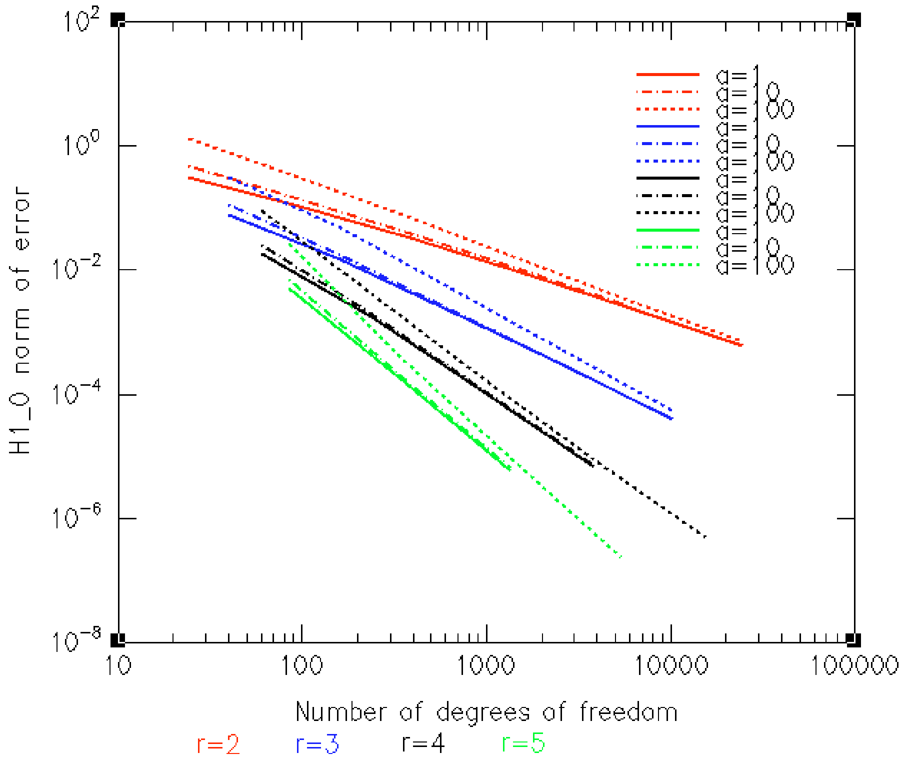

Figure 2: H_0^1 error versus number of degrees of freedom.

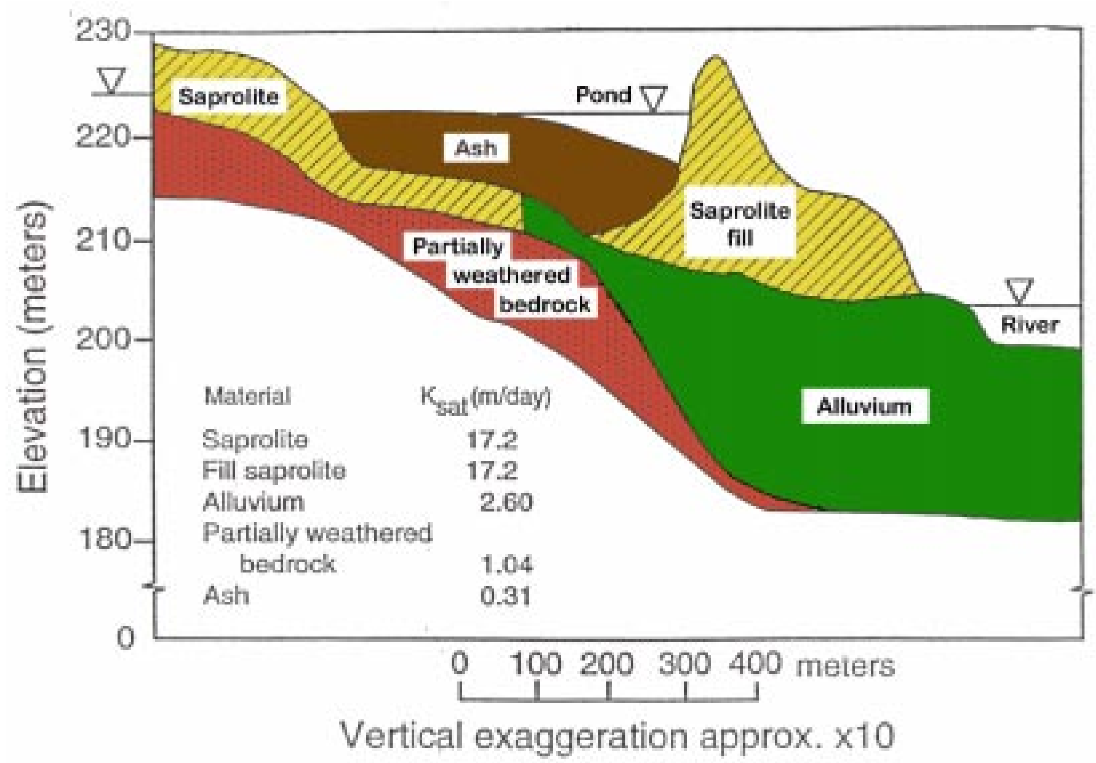

Figure 3: Geology of the L-site.

conditions except for the top boundary , $_D$, where we impose the following condition:

$$p(x, y) = y \quad \forall (x, y) \in \, _D.$$

The pressure and velocity fields are shown in Fig.6. In this example, a quadratic approximation has been used. In [4], it was shown that the conforming finite element method yields non-physical behavior, in particular streamlines would end on the no-flow boundaries. We can see that the DG method does not have this problem. Kaasschieter used the mixed finite element method, which involved solving a saddle-point problem.

We have computed the time it takes for a particle of water to reach the boundary of the domain. This time is denoted residence time, and we looked at four different starting points in the mesh. The results are tabulated in Table 4. Very similar results were obtained in [4]. The streamlines are shown in Fig. 7 and Fig.8.

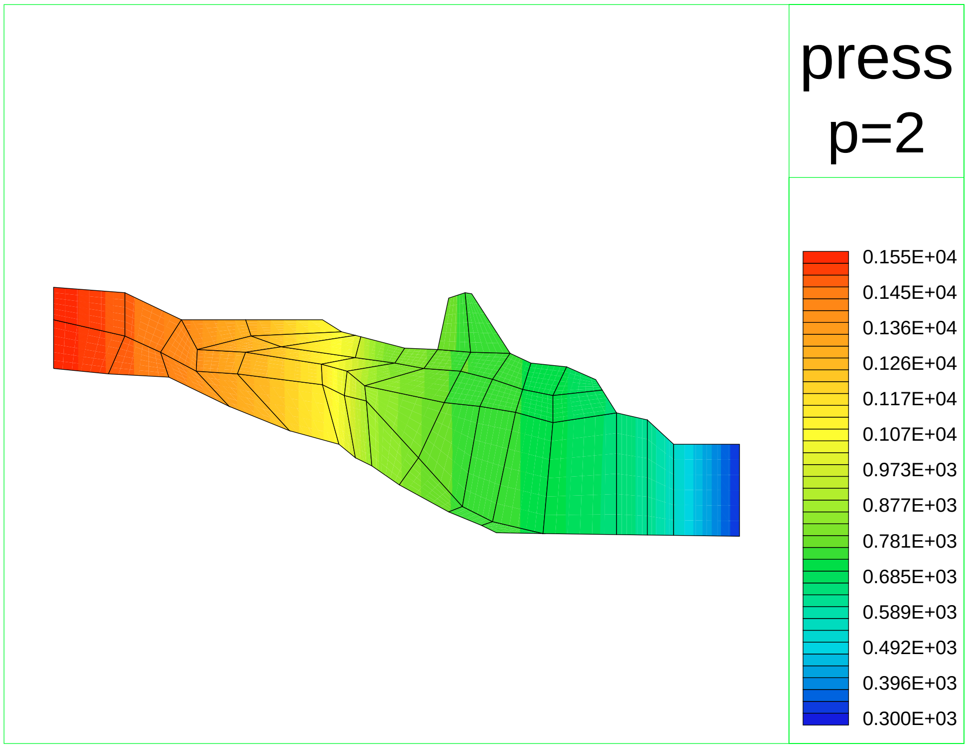

Figure 4: Quadratic approximation of pressure field.

	r=2		r=3	
(x, y)	$N = 85$	$N = 340$	$N = 85$	N=340
(100,0)	0.28×10^{11}	0.39×10^{11}	0.34×10^{11}	0.33×10^{11}
$(100, -200)$	0.49×10^{12}	0.63×10^{12}	0.14×10^{12}	0.44×10^{12}
(1500,0)	0.27×10^{11}	0.27×10^{11}	0.31×10^{11}	0.27×10^{11}
(1500,-450)	0.51×10^{12}	0.30×10^{12}	0.29×10^{12}	0.27×10^{12}

Table 4: Residence times.

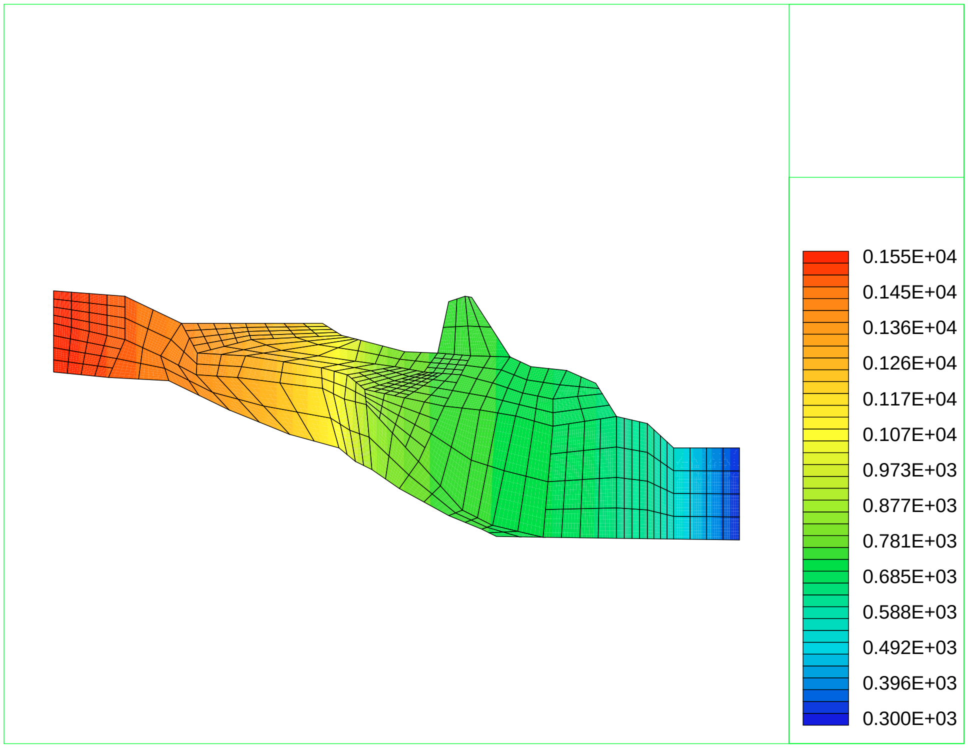

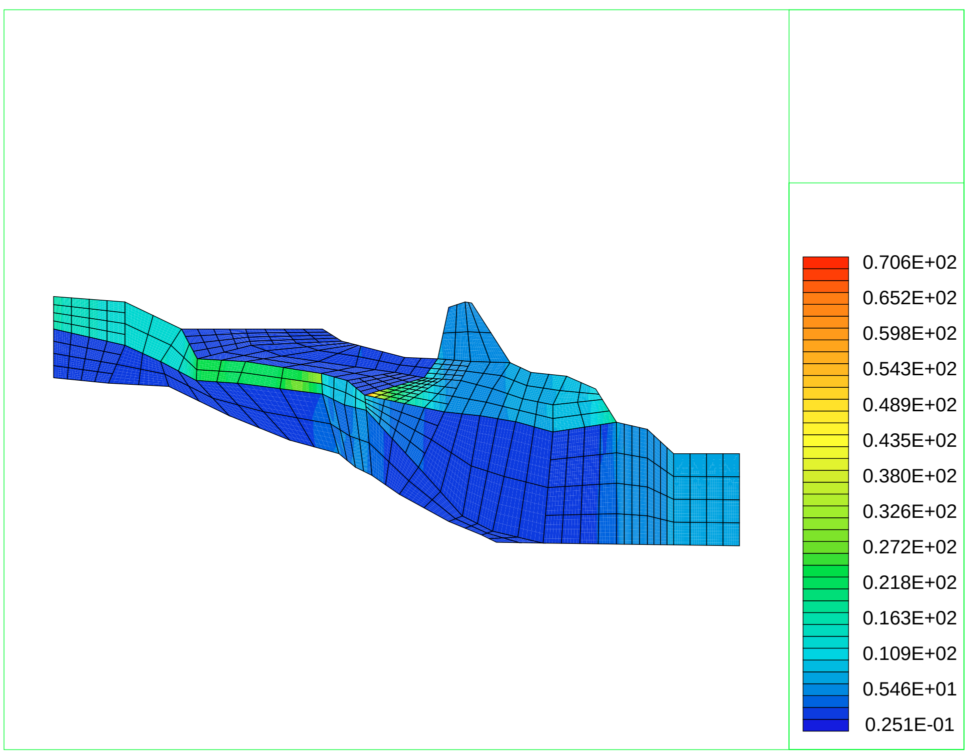

Figure 5: Pressure field and velocity field: *hp* approximation.

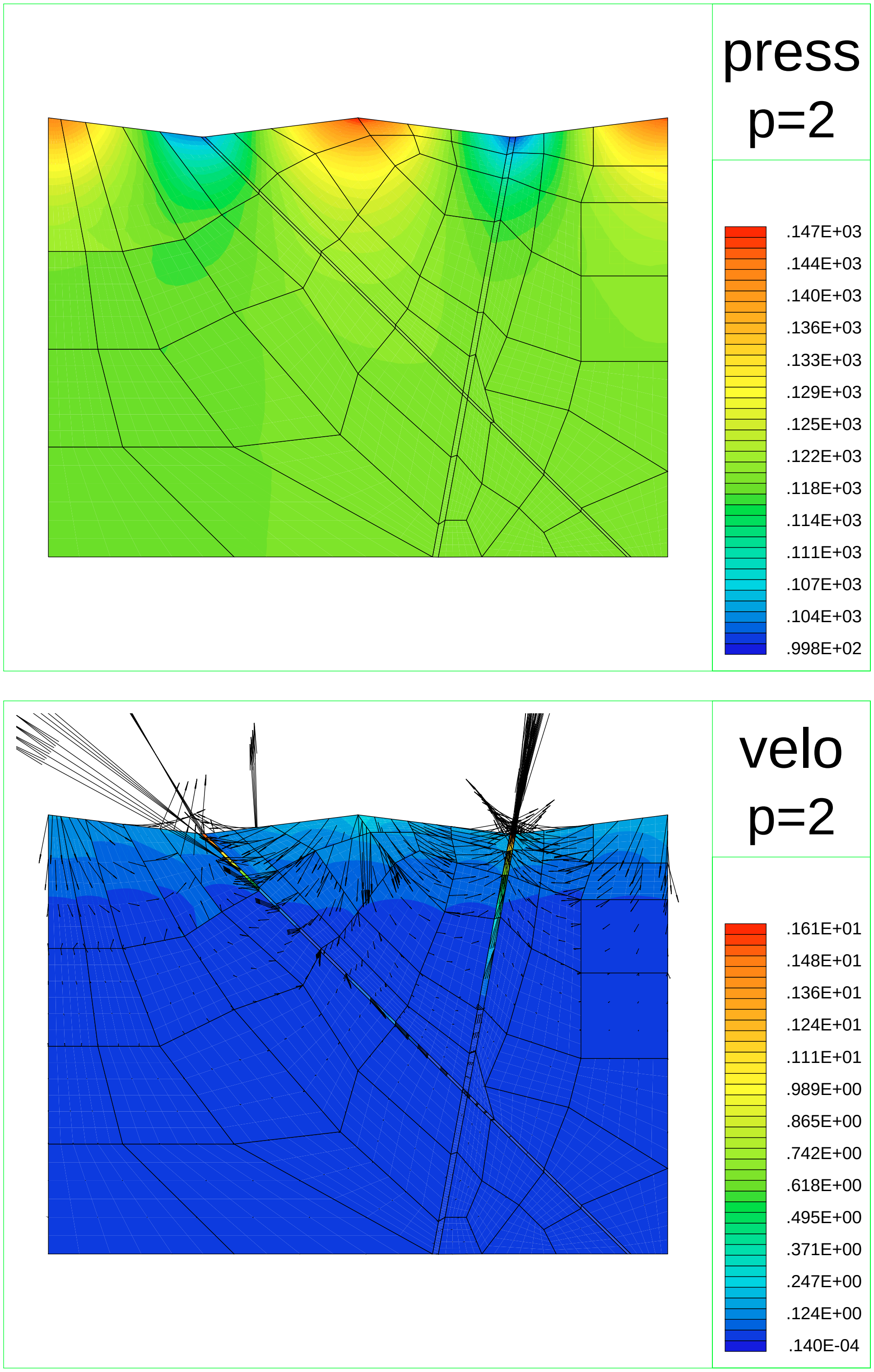

Figure 6: Pressure field and velocity field: quadratic approximation.

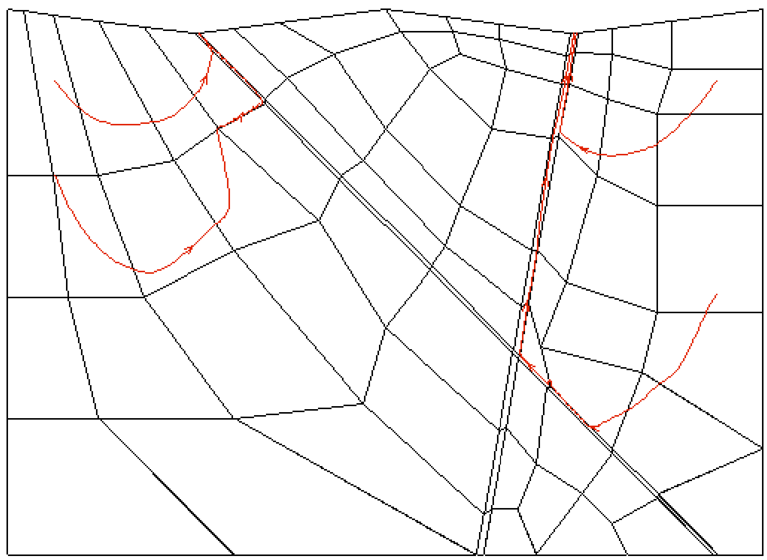

$r = 2$

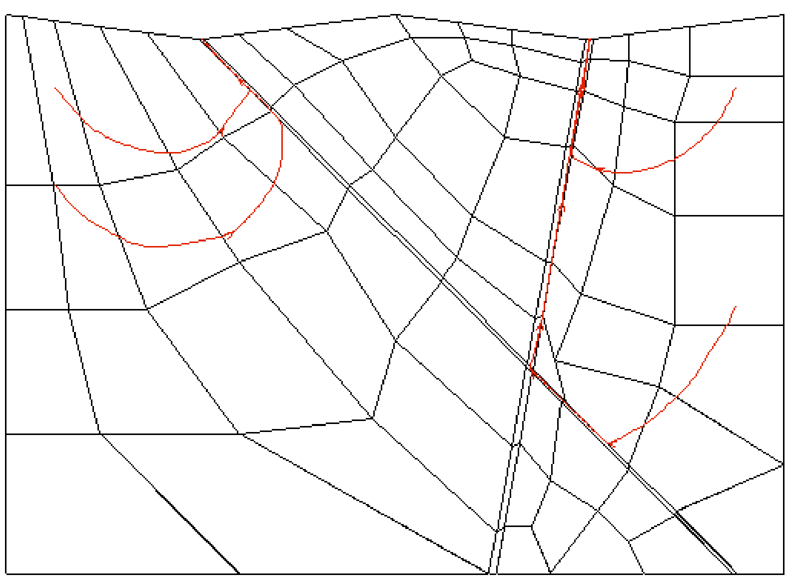

$r = 3$

Figure 7: Particle tracking on a coarse mesh.

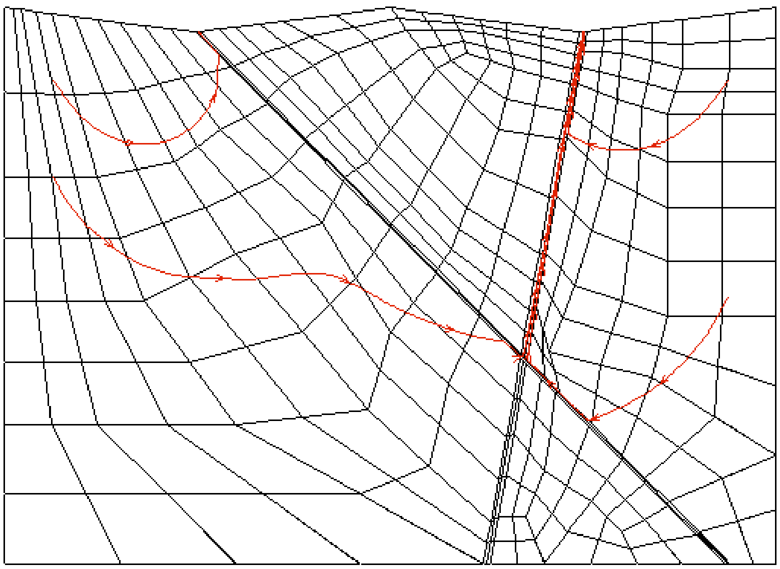

$r = 2$

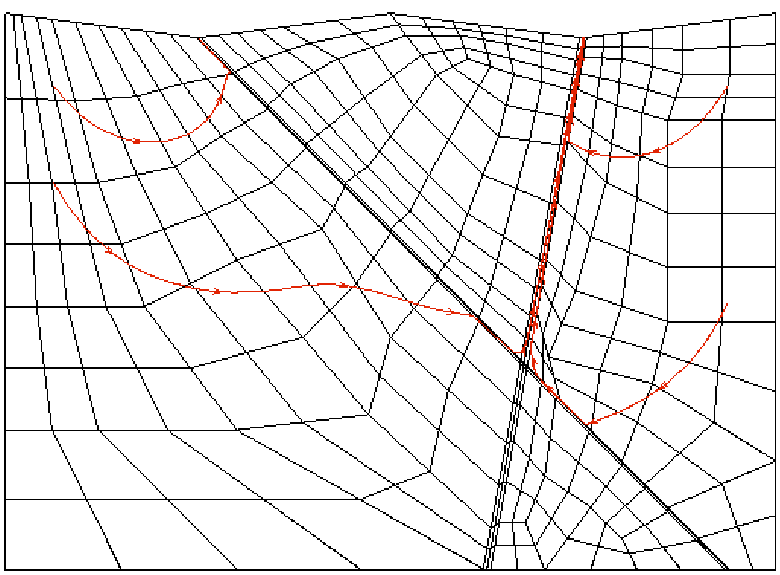

$r = 3$

Figure 8: Particle tracking on a refined mesh.

4 Error estimation

We investigate the two types of error estimators derived in the previous chapter. The true solution is given by

$$p_{ex}(x,y) = x^2(x^2-1)y^2(y^2-1)(e^x-1)(e^y-1) \quad \forall (x,y) \in (0,1)^2$$

The material has a constant permeability equal to 1. Dirichlet boundary conditions are assumed. The initial domain consists of four quadrilateral elements. Fig.10 shows the true solution and the computed DG solution of quadratic approximation. We have

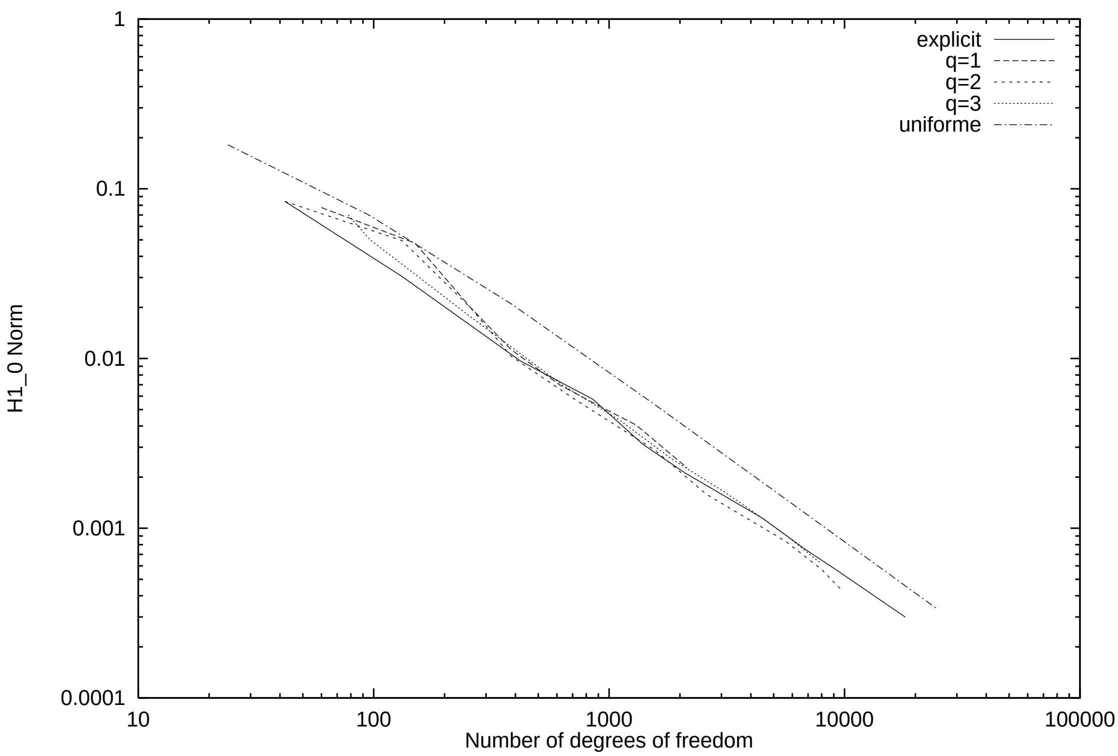

Figure 9: H_0^1 error versus number of degrees of freedom.

used the two types of *a posteriori* error estimates as error indicators, and Fig.9 shows that for a given accuracy both error indicators behave the same. Using h adaptivity, the solution is computed for an amount of work that is less important.

We investigate the effectivity index defined as follows

$$\chi_{H_0^1} = \frac{\|\Phi_h\|}{\|p - P^{DG}\|},$$

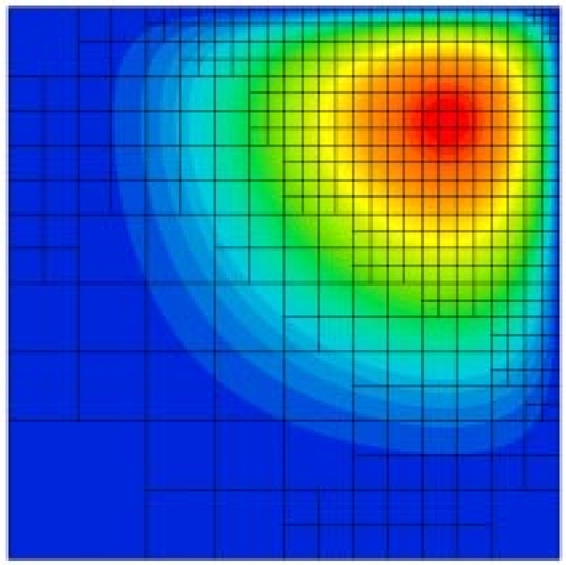

true solution

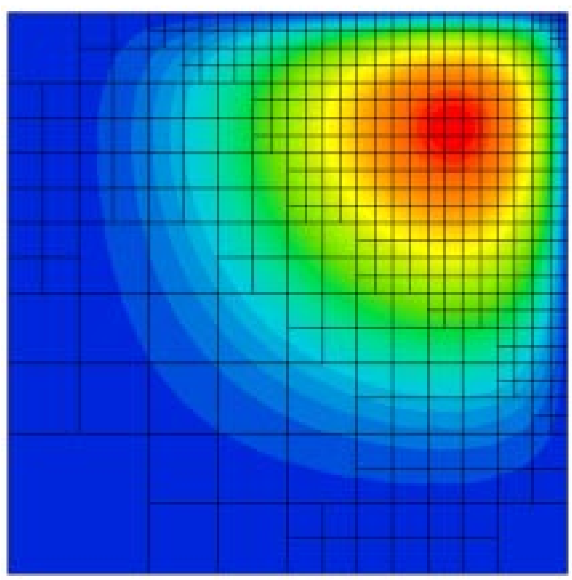

computed solution $r = 2$

Figure 10: Exact and h-adaptive solutions.

where ϕ_h is the discrete solution of the weak problem:

$$\sum_{j=1}^{N_h} \int_{E_j} (K\nabla\Phi_h \cdot \nabla v) = L(v) - a_{NS}(P^{DG}, v), \quad \forall v \in \mathcal{D}_{r+q}(\mathcal{E}_h)$$

We will show in a future paper the derivation of this error estimator. In Fig.11, we note that the effectivity index converges to 1 for certain values of enrichment.

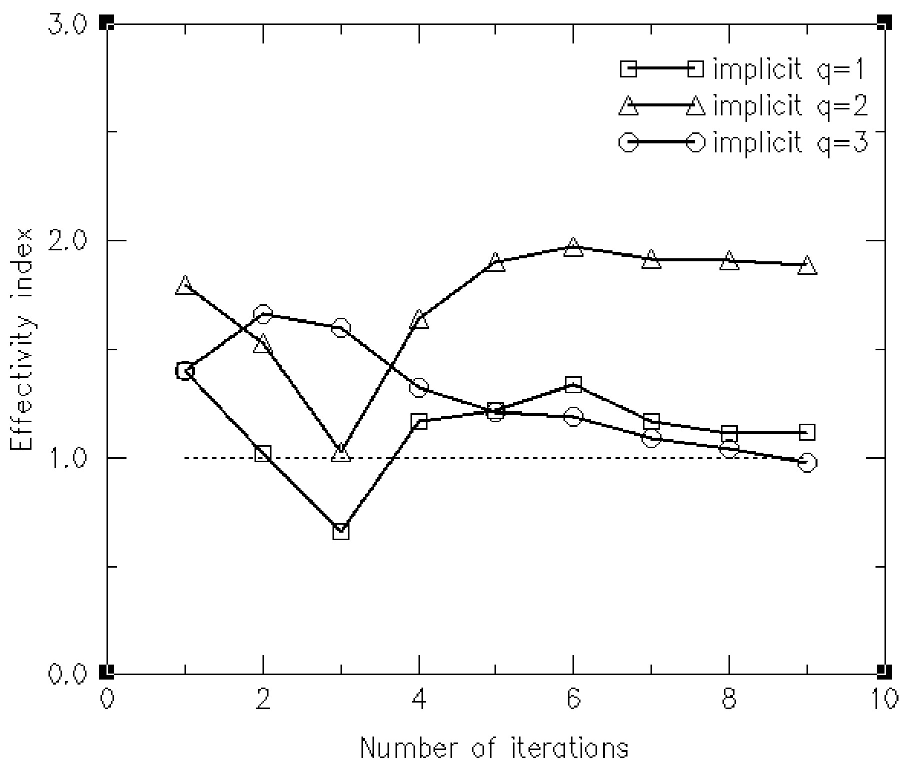

Figure 11: Effectivity indices.

5 Conclusion

The DG method is easier to implement than the NIPG (Nonsymmetric Interior Penalty Galerkin) method and the NCG (Nonsymmetric Constrained Galerkin) method. Numerical experiments show that the DG method handles the rough coefficients problems very well. Non-physical behavior is not obtained as it is the case for more conforming finite element methods. Another advantage of the DG method is that adaptivity is easily implemented. *A posteriori* error estimates for the DG method are proved in a future paper.

References

[1] I. Babuska and M. Suri. The h-p version of the finite element method with quasiuniform meshes. *Mathematical Modeling and Numerical Analysis*, 21(2):199–238, 1987.

[2] I. Babuska and M. Suri. The optimal convergence rate of the p-version of the finite element method. *SIAM J.Numer. Anal.*, 24(4), August 1987.

[3] C.E.Baumann. *An h-p adaptive discontinuous finite element method for computational fluid dynamics*. PhD thesis, The University of Texas at Austin, 1997.

[4] E.F.Kaasschieter. Mixed finite elements for accurate particle tracking in saturated groundwater flow. *Advances in Water Resources*, 18(5):277–294, 1995.

[5] J.T.Oden, I.Babuska, and C.E. Baumann. A discontinuous hp finite element method for diffusion problems. *Journal of Computational Physics*, 146:491–519, 1998.